 MCB, vol.5, no.4, pp.247-257, 2008

Short-Term Shear Stress Induces Rapid Actin Dynamics in Living Endothelial Cells

Colin K. Choi* **and Brian P. Helmke*,†**

Abstract: Hemodynamic shear stress guides a variety of endothelial phenotype characteristics, including cell morphology, cytoskeletal structure, and gene expression profile. The sensing and processing of extracellular fluid forces may be mediated by mechanotransmission through the actin cytoskeleton network to intracellular locations of signal initiation. In this study, we identify rapid actin-mediated morphological changes in living subconfluent and confluent bovine aortic endothelial cells (ECs) in response to onset of unidirectional steady fluid shear stress (15 dyn/cm^2). After flow onset, subconfluent cells exhibited dynamic edge activity in lamellipodia and small ruffles in the downstream and side directions for the first 12 min; activity was minimal in the upstream direction. After 12 min, peripheral edge extension subsided. Confluent cell monolayers that were exposed to shear stress exhibited only subtle increases in edge fluctuations after flow onset. Addition of cytochalasin D to disrupt actin polymerization served to suppress the magnitude of flow-mediated actin remodeling in both subconfluent confluent EC monolayers. Interestingly, when subconfluent ECs were exposed to two sequential flow step increases (1 dyn/cm^2 followed by 15 dyn/cm^2 12 min later), actin-mediated edge activity was not additionally increased after the second flow step. Thus, repeated flow increases served to desensitize mechanosensitive structural dynamics in the actin cytoskeleton.

Keyword: mechanotransduction, endothelium, shear stress, actin cytoskeleton, cytochalasin D

* Department of Biomedical Engineering and Robert M. Berne Cardiovascular Research Center, University of Virginia, Charlottesville, Virginia, USA

† Corresponding author. Phone: +1 434-924-1726; Fax: +1 434-982-3870; Email: helmke@virginia.edu

1 Introduction

The endothelium, a one-cell-thick inner lining of blood vessels that is formed by endothelial cells, serves numerous important vascular functions, and many of these are influenced by mechanical cues associated with hemodynamic shear stress (1, 2). In vascular pathology, atherosclerosis is characterized by lesion formation on the artery wall, suggesting that the endothelium plays a major role in disease development (3, 4). Moreover, the locations of atherogenesis in the arterial tree correlate with the spatial distribution of fluid shear stress (5, 6). Thus, the need for a clear understanding of how blood flow affects the biology of endothelial cells is well-recognized.

The luminal surface of endothelial cells (ECs) is the boundary that is exposed to blood flow; thus, it is continually subjected to hemodynamic shear stress. In vitro shear stress studies have shown that endothelial cells respond dynamically to specific patterns of hemodynamic forces to produce functional biochemical agents, to regulate gene expression, and to rearrange their morphology and cytoskeleton (7-11). In addition, many of the flow-mediated reactions are exquisitely orchestrated both temporally and spatially (12). A decentralized mechanotransduction model proposes that the mechanical load of shear stress is transmitted along the cytoskeleton and is distributed to various intracellular locations (1). The resultant biochemical signals from both local and remote sites may then be integrated to yield flow-induced endothelial adaptation.

Without intact cytoskeleton, mechanotransduction would be depressed or even eliminated if the structure were required to facilitate force transmission. Thus, cytoskeletal mechanics and dynamics continue to be major focal points in un-

derstanding how endothelial cells coordinate mechanical forces and signaling pathways systematically. While actin microfilaments, vimentin intermediate filaments, and tubulin microtubules make up the cytoskeleton that undergoes flow-induced reorganization, actin has been most widely studied (13-17). The importance is due to the physical connections that actin filaments make to potential mechanotransduction sites, including focal adhesions and the nucleus (18, 19). Indeed, numerous flow-mediated endothelial responses, including shape realignment, focal adhesion remodeling, and gene expression regulation are inhibited when actin polymerization is disrupted (1).

The overall goal of this work was to test the hypothesis that the actin cytoskeleton serves as a primary force-affected element that the cell employs from the onset of flow to sense fluid shear stress. GFP-actin and high resolution 4-D microscopy enabled fast, real-time visualization of actin-mediated morphology changes in living endothelial cells.

2 Materials and Methods

2.1 Cell Culture and Transfection with GFP-actin

Bovine aortic endothelial cells (ECs), passages 10-14, were cultured in complete growth medium consisting of Dulbecco's Modified Eagle's Medium (Invitrogen, Carlsbad, CA) supplemented with 10% heat-inactivated newborn calf serum (HyClone, Leesburg, VA), 2 mM L-glutamine (Invitrogen), 50 IU/ml penicillin (Invitrogen), and 50 μg/ml streptomycin (Invitrogen). Cells were maintained in a 100% relative humidity atmosphere of 95% air and 5% CO_2 at 37 ˚C. Cells were transfected for 2.5 h with pEGFP-actin (Clontech, Mountain View, CA) in Opti-MEM I (Invitrogen) using a liposomal method (Lipofectin, Invitrogen). Cells were allowed to recover for 24 h in complete medium and were plated onto sterile No. 1.5 glass coverslips (Bioptechs, Butler, PA) coated with red fluorescent microspheres (0.1-μm diameter, FluoSpheres, Molecular Probes, Eugene OR) that served as substrate fiducial marks during time-lapse imaging.

2.2 Shear Stress Apparatus

Coverslips with transfected cells at the desired area density were assembled into a parallel plate flow chamber (Bioptechs) that was connected to a closed flow loop, as described previously (20, 21). The perfusion medium consisted of complete growth medium without phenol red and supplemented with 25 mM HEPES buffer (Invitrogen). Volumetric flow rate in the chamber was driven by gravitational force and adjusted to generate wall shear stress of 15 dyn/cm^2. The objective lens and the flow chamber were maintained at 37 ˚C. In some experiments, a syringe pump (Harvard Apparatus, Holliston, MA) was switched into the flow loop to set wall shear stress magnitude at 1 dyn/cm^2. In separate experiments, 0.05 μM cytochalasin D (Sigma-Aldrich, St. Louis, MO) was introduced in the perfusion medium.

2.3 3-D Time-lapse Image Acquisition

Wide-field fluorescence optical sections were acquired using a DeltaVision restoration microscopy system (Applied Precision, Issaquah, WA). Image stacks with thickness 3-4 μm and z-interval 0.2 μm were acquired every 2 to 3 min during an experiment. The image acquisition protocol was divided into three phases: 9-14 min without flow; 30 min with flow; and 9-14 min without flow. During the second phase with flow, the wall shear stress either was maintained at 15 dyn/cm^2 for 30 min or was started at 1 dyn/cm^2 for 12 min and was stepped up to 15 dyn/cm^2 for 18 min. One to three cells were examined per coverslip.

2.4 Deconvolution and Image Analysis

In order to reposition out of focus light, 3-D images at each time point were deconvolved using *SoftWoRx* software (Applied Precision) as described previously (20, 21) to reposition out of focus light (22). In order to reduce effects of shot noise in the low light level optical sections, a 3x3-pixel median filter was implemented using *MATLAB* (MathWorks, Natick, MA). Stacks of optical sections were then restored as volumetric projections. The area of GFP-actin in the volume

projections was measured by manually outlining the fluorescence border using *Scion Image* (Scion Corporation, Frederick, MD). Time-lapse movies were generated using *ImageJ* software (23). The spatial directionality of actin area dynamics in the cell was scored as follows. Outlined cell images were divided into four symmetric regions, and the differences of actin areas in these regions at consecutive time points were accumulated to find average increases or decreases within an interval. The centroid of the reference image at the earlier time point was chosen as the foci of the quadrants. Analysis of variance (ANOVA) with repeated measures and Tukey-Kramer pairwise comparisons were performed in MINITAB (Minitab Inc.), and means were considered significantly different at the 95% confidence level.

3 Results

3.1 Actin Reorganization in Subconfluent and Confluent ECs Under Shear Stress

Using 4-D fluorescence microscopy, GFP-actin mediated morphological changes induced by flow were analyzed both qualitatively and quantitatively. In the absence of flow, random bursts of actin polymerization existed around the periphery of subconfluent ECs (**Figure 1A**). These bursts were qualitatively defined as balloon-like, actin-containing projections at the cell boundary, including lamellipodia and outward edge expansions. When subconfluent ECs were exposed to fluid shear stress, they exhibited synchronized bursts of actin polymerization activity within minutes of flow onset (**Figure 1B**). The F-actin edge structures formed, enlarged, and retracted transiently on a minutes time scale. During continued flow, actin bursts subsided and peripheral edge extension ceased. Direct comparison of images across time in colored overlays demonstrated that actin filaments and stress fibers were elongated, shortened, and displaced laterally during the first few minutes after flow onset (**Figure 1C**).

In order to determine whether flow onset induced a systematic cell spreading response, the projected cell area derived from GFP-actin fluorescence was tracked relative to the area at flow onset

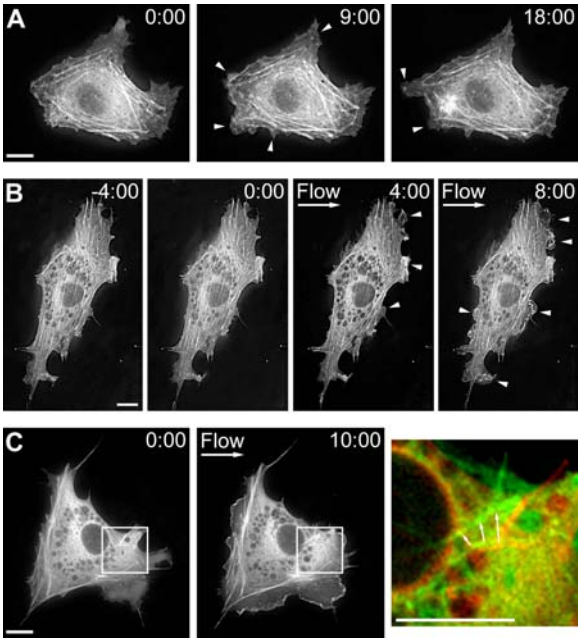

Figure 1: GFP-actin boundary activity in a subconfluent EC layer. Arrows indicate peripheral actin bursts or remodeling. (A) No-flow control. (B) Before and after flow onset at t=0:00 (left to right). (C) After flow onset at t=0:00. Inset demonstrates displacement of basal stress fibers (arrows) from t=0:00 (red) to t=10:00 (green). Time=mm:ss. Bar=10 μm.

(Time = 0 min, **Figure 2A**). Prior to the flow onset, the relative cell area remained constant near unity. Within 2 min after flow onset, the relative cell area increased rapidly to 1.03 ± 0.02. This upward trend was continued until a maximum of 1.11 ± 0.05 was reached at 12 min. After this time, normalized area decreased linearly at a rate of -0.0030 min^{-1} (R^2 = 0.97). During at least the first 30 min of flow, the projected cell area was significantly larger than cells maintained under no-flow conditions ($p<0.05$, n=7-10). In contrast to the response to flow onset, cells maintained under no-flow condition maintained a constant projected area; a linear regression demonstrated that the rate of change of relative area was -0.0008 min^{-1}, which was not significantly different from zero (n=10).

In order to determine whether flow-induced, actin-mediated morphology changes that were

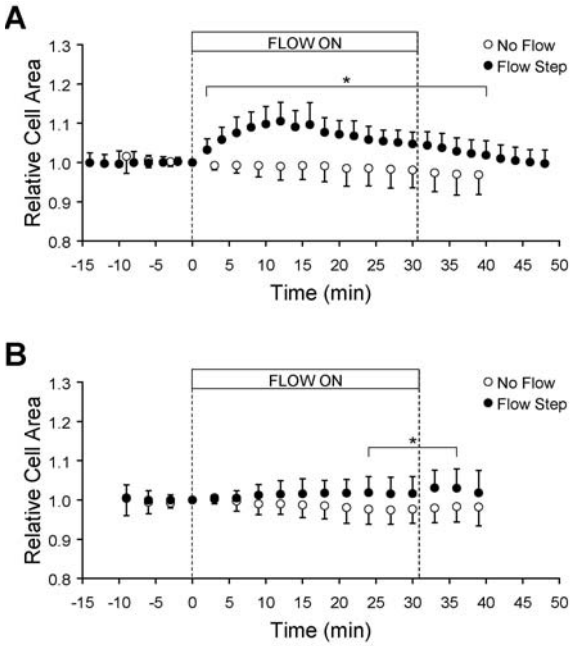

Figure 2: Cell area (mean ± SD) relative to t=0 min indicated by GFP-actin in (A) subconfluent and (B) confluent EC layers exposed to no-flow (open circles) or to steady unidirectional flow during the indicated interval (closed circles) at a wall shear stress of 15 dyn/cm^2. *Significantly different than no-flow ($p<0.05$).

similar to those observed in subconfluent ECs also occur in a more physiological condition, confluent monolayers were examined. Prior to the onset of shear stress, projected cell area was constant with time. In contrast to the behavior of subconfluent ECs, this relatively steady area was maintained at a level similar to control after flow onset. Over a longer time scale, confluent ECs did gradually increase in area, reaching 1.02±0.04 after 24 min (n=9-11). The relative cell area in monolayers maintained under no-flow conditions remained constant (linear regression slope of -0.0006 min^{-1}).

Visual analysis of ECs in confluent monolayers revealed subtle morphological dynamics. Although these ECs were tightly surrounded by adjacent cells (verified with vascular endothelial cadherin immunostaining; data not shown), undulating edge fluctuations occurred (**Figure 3**). These wavy structures were not large enough to induce an area change, and they were not observed in subconfluent layers. ECs in confluent monolayers also produced small random actin bursts throughout the course of experiments; however, dominant flow-induced actin bursts were not detected. Moreover, seven of nine cells under no-flow conditions either elongated or spread to reshape while only four of eleven cells exposed to the flow condition displayed similar shape remodeling. This observation indicates that shear stress enables cells to maintain shape and architecture.

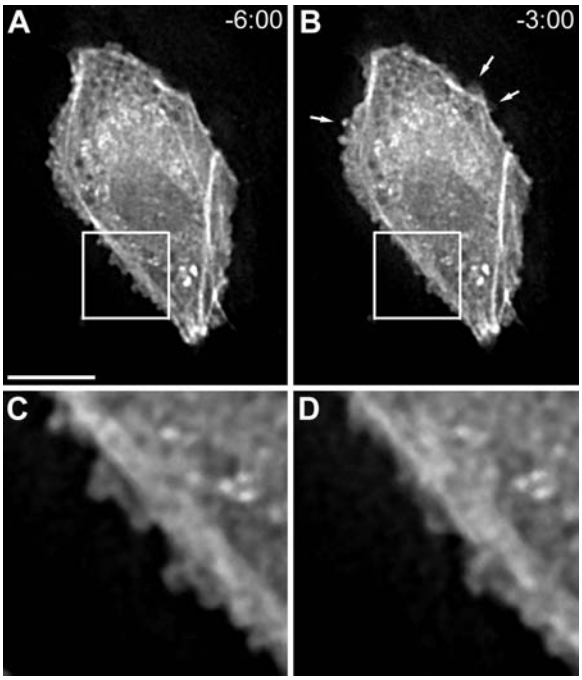

Figure 3: GFP-actin boundary activity in a confluent EC layer (A) 6:00 before and (B) 3:00 before flow onset. Arrows indicate locations of peripheral actin bursts. (C) and (D) are insets from (A) and (B), respectively, that illustrate subtle edge position fluctuations during the 3-min interval. Time=mm:ss. Bar=10 μm.

3.2 Shear Stress-Mediated Actin Dynamics in the Presence of Cytochalasin D

To examine whether disruption of actin dynamics would affect flow-induced actin morphology responses, ECs were treated with cytochalasin D to inhibit actin polymerization. In the presence of cytochalasin D under no-flow conditions, ECs

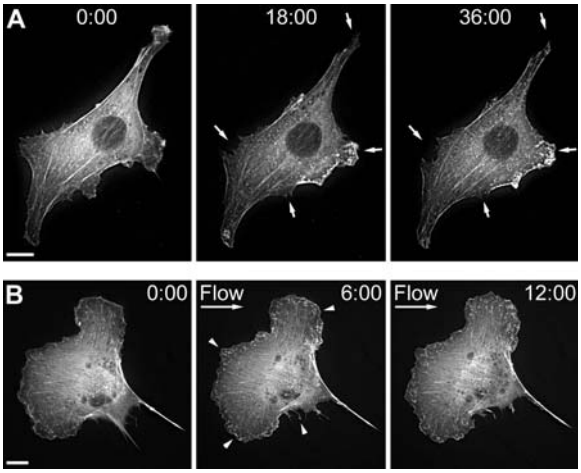

Figure 4: GFP-actin remodeling in a subconfluent EC layer treated with cytochalasin D at t=0:00. White arrows indicate filament shortening, edge retraction, or speckle formation. Green arrows follow centripetal motion of actin aggregate that was formed at a leading edge. (A) No-flow control after addition of cytochalasin D. (B) After onset of flow at t=0:00 with medium containing cytochalasin D. Time=mm:ss. Bar=10 μm.

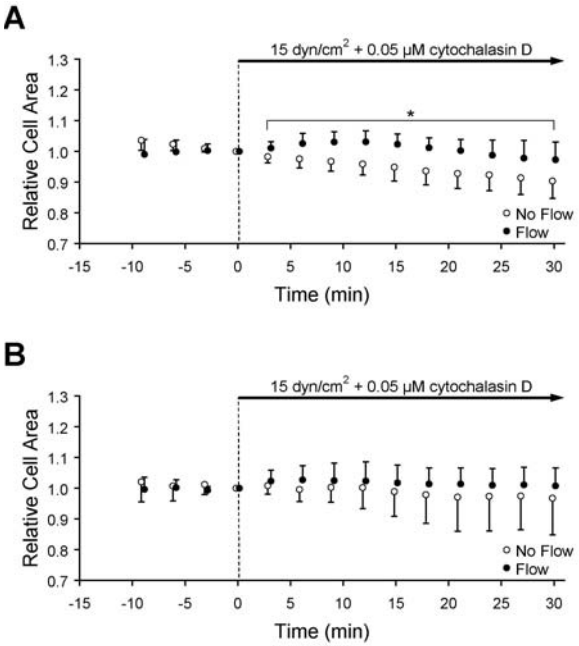

Figure 5: Cell area (mean $\pm$ SD) relative to t=0 min indicated by GFP-actin in (A) subconfluent and (B) confluent EC layers. At t=0 min, either cytochalasin was added under no-flow conditions (open circles) or simultaneously with the onset of steady unidirectional flow (closed circles) at a wall shear stress of 15 dyn/cm^2. *Significantly different than no-flow ($p<0.05$).

in subconfluent layers slowly retracted their edges via actin filament bundle shortening and boundary displacement. In some cases, the cell periphery became concentrated with actin, and the fragments of actin moved centripetally in time (**Figure 4A**). Moreover, speckles of actin with no clear traffic pattern were developed in the cytoplasm as early as 3 min after the introduction of cytochalasin D. After flow onset, cytochalasin D suppressed the degree of synchronized actin bursts at the cell boundary (**Figure 4B**). In a manner similar to the no-flow condition, actin speckles emerged within minutes of flow, and in some cells, they were heavily localized in the active periphery regions. In addition, cells that were treated with cytochalasin D and flow exhibited large displacements of actin stress fibers, especially when edges were retracting quickly.

The projected area of ECs in subconfluent layers treated with cytochalasin D decreased linearly at a rate of -0.0030 min^{-1} (measured from 12 to 39 min, R^2 = 0.995, **Figure 5A**). The onset of flow caused a rapid, small magnitude increase in relative cell area, reaching a peak value of 1.03$\pm$0.04 after 12 min. In a manner similar to untreated cells, the relative cell area decreased gradually after 12 min despite sustained flow. A linear trend line fit from 12 to 39 min indicated that the area decreased at -0.0034 min^{-1} (R^2 = 0.995).

Qualitative analysis of confluent EC layers demonstrated that these cells exhibited subtle edge fluctuations that were similar to those in the absence of cytochalasin D. Also, eight of nine confluent cells under no-flow conditions with cytochalasin D underwent a shape change, which included elongation and spreading that decreased the mean shape index of the cells from 0.44$\pm$0.08 at t=0 to 0.38$\pm$0.09. In cells that were exposed to shear stress, shape changes were not observed; however, seven of nine cells exhibited small synchronized actin bursts.

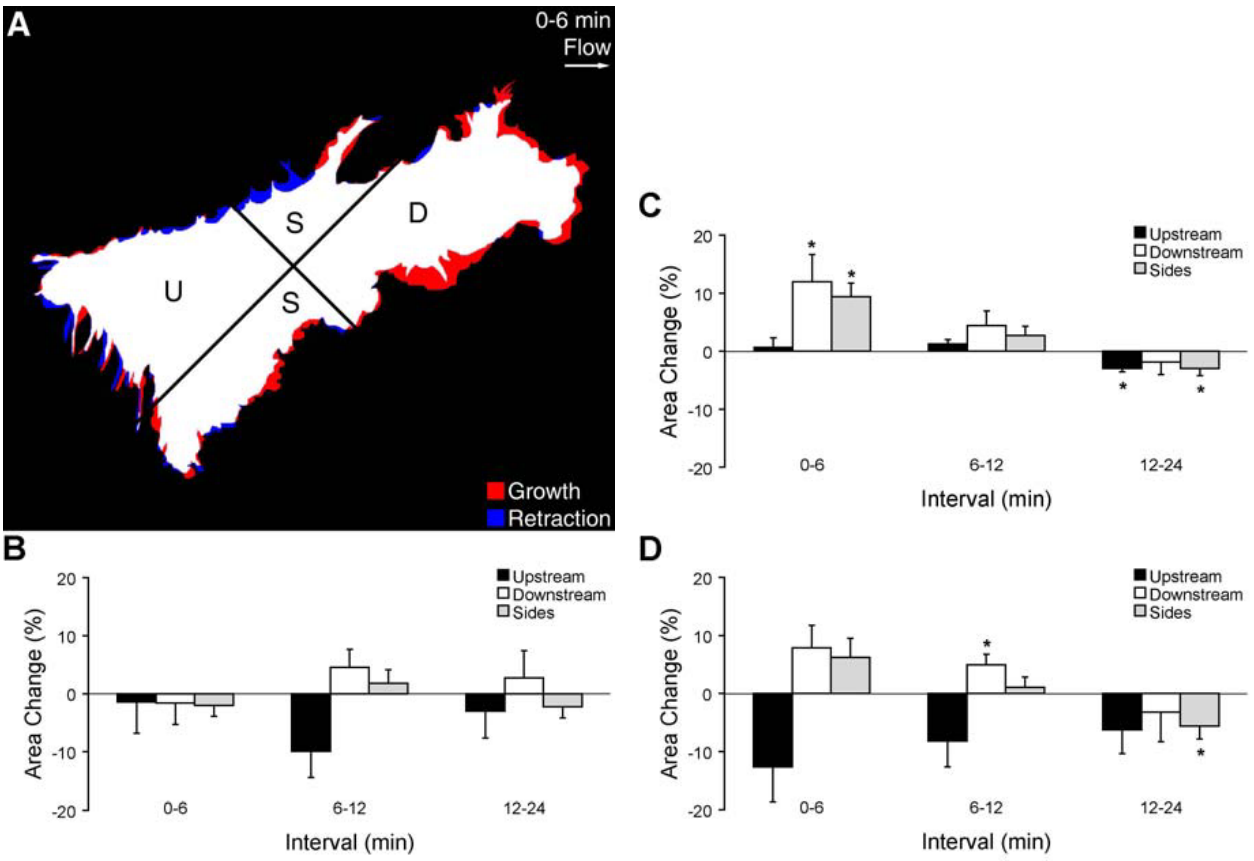

Figure 6: Directionality of GFP-actin area change in a subconfluent EC layer. (A) Schematic overlay of GFP-actin images at the beginning and end of a 6-min interval after flow onset, illustrating area growth (red) and retraction (blue). White indicates areas that did not change in quadrants oriented upstream (U), downstream (D), or towards the sides (S) with respect to the flow direction. (B) Area changes (mean±SE) during consecutive 6-min intervals without flow. (C) Area changes during consecutive 6-min intervals after onset of unidirectional steady flow at t=0 min. (D) Area changes after onset of flow with medium containing cytochalasin D. *Significantly different than zero ($p<0.05$).

Between 6 and 21 min after the application of cytochalasin D, the ECs in confluent monolayers under no-flow conditions decreased their relative cell area (**Figure 5B**). After 21 min with cytochalasin D, the relative cell area remained constant at 0.96±0.11. Area changes in the presence of drug were highly variable, as indicated by increased standard deviation. When confluent monolayers were exposed to shear stress in the presence of cytochalasin D, relative cell area increased to 1.02±0.04 after 3 min. Relative cell area was significantly greater than that in the absence of flow ($p<0.05$, n=9-11) but was not greater than that of cells not treated with cytochalasin D.

3.3 Directionality of Flow-induced Actin Bursts

The spatial distribution of these flow-induced actin bursts were quantitatively analyzed by plotting relative area change in quandrants designated upstream, downstream, or side-to-side relative to the direction of shear stress (**Figure 6A**). ECs in subconfluent layers under no-flow conditions maintained constant projected area as a function of time in all quadrants (**Figure 6B**). During the first 6 min after flow onset, flow-induced actin bursts were more prominent in the downstream and side directions compared to the upstream direction, as demonstrated by a significant increase

in area in those regions (**Figure 6B**, p<0.05, n=10). During the next 6-min interval, the area changes in all regions decreased, consistent with maintenance of cell area. During the interval 12-24 min after flow onset, area decreased significantly in the upstream and side regions (p<0.05, n=7) but not in the downstream region, suggesting that cells were establishing a polarity oriented parallel to the shear stress direction. The directionality of flow-induced actin bursts in the presence of cytochalasin D exhibited similar spatial and temporal trends as in untreated cells (**Figure 6D**), but the magnitude of area changes was generally smaller. A clear trend towards directional polarity (increased area in downstream and side regions accompanied by decreased area in the upstream region) was apparent during all intervals. During the interval 6-12 min after flow onset, area increased significantly in the downstream region (p<0.05, n=10) and was maintained during the subsequent 12-min interval. During the interval 12-24 min after flow onset, area decreased significantly in the side regions, consistent with shape elongation parallel to the flow axis.

3.4 Desensitization of Flow-induced Actin Response

Since it is not clear whether mechanically-triggered changes in actin dynamics represent an all-or-none response, we asked whether ECs are capable of sensing a second change in flow while they are responding to the initial flow step. To address this question, subconfluent EC layers were first exposed to shear stress at 1 dyn/cm^2. After 12 min, the time point at which the maximum mean area occurs, a step increase in shear stress to 15 dyn/cm^2 was imposed. Time-lapse movies revealed that ECs in subconfluent layers responded in a less dramatic fashion to 1 dyn/cm^2 shear stress than they did to 15 dyn/cm^2 alone. After flow onset, previously quiescent borders developed spatially concentrated GFP-actin and subsequently expanded then subsided in time. More importantly, a second step increase of 15 dyn/cm^2 did not cause additional flow-mediated actin bursts (**Figure 7**).

The relative cell areas exhibited two key features

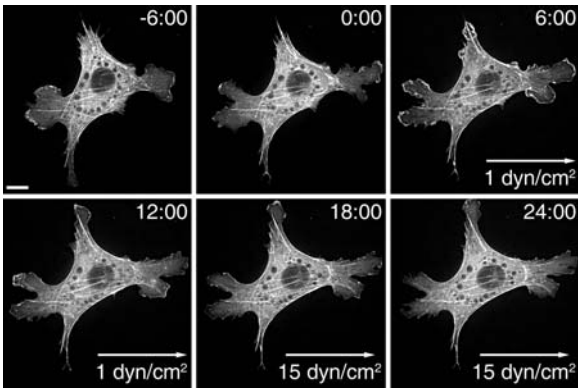

Figure 7: GFP-actin boundary activity in a subconfluent EC layer before and after onset of steady unidirectional shear stress to 1 dyn/cm^2 at t=0 min followed by a second increase to 15 dyn/cm^2 at t=12 min. Arrows indicate locations of peripheral actin bursts or remodeling. Time=mm:ss. Bar=10 μm.

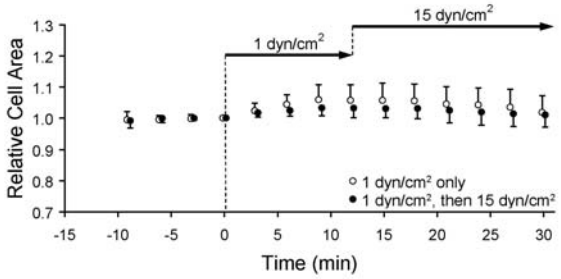

Figure 8: Cell area (mean $\pm$ SD) relative to t=0 min indicated by GFP-actin area in a subconfluent EC layer exposed to a single step onset of shear stress to 1 dyn/cm^2 at t=0 min (open circles) or to 1 dyn/cm^2 at 0 min followed by a step increase to 15 dyn/cm^2 at t=12 min (closed circles).

(**Figure 8**). First, the degree of flow-induced actin bursts was shear stress magnitude dependent. Compared to ECs exposed to 15 dyn/cm^2 (Figure 2A), the relative cell area increased less in response to onset of shear stress at 1 dyn/cm^2. At 12 min after onset of 1 dyn/cm^2, the maximum relative cell area was 1.04$\pm$0.04, which was significantly less than the value reached after onset of 15 dyn/cm^2 (p<0.05). Second, increasing the shear stress from 1 dyn/cm^2 to 15 dyn/cm^2 did not induce a second transient increase in relative

cell area. The relative cell area of cells exposed to double step changes followed the same temporal pattern as that of cells exposed to a single step onset of 1 dyn/cm^2, increasing during first 12 min and returning to the baseline afterwards.

4 Discussion

In the present study, the actin cytoskeleton in endothelial cells was reorganized rapidly in response to shear stress, suggesting that the mechanical cue from fluid shear stress was a direct regulator in promoting structural remodeling. Onset of shear stress has been shown to induce rapid intermediate filament displacement and strain focusing at discrete locations, suggesting that applied forces are distributed in the intracellular space (21, 24). Over a time scale of hours to days, the actin cytoskeleton realigns in the direction of flow (2, 8), yet it is not yet known how the cell employs actin in its force-sensing mechanism from the onset of flow. Most other studies reporting flow-mediated actin reorganization have reported structure by immunostaining cells fixed at hourly or 30-min intervals. Thus, there existed a gap in knowledge regarding how early and in what way endothelial cells adapt the actin cytoskeleton when a change in the flow environment is introduced. In this study, GFP-actin enabled continuous visualization of the actin cytoskeleton in living endothelial cells during and after onset of hemodynamic shear stress.

After the onset of shear stress, ECs in subconfluent layers exhibited synchronized, transient actin polymerization bursts, which included lamellipodia and small peripheral extensions. Although it is unclear whether this phenomenon is a direct flow-sensing mechanism or a prerequisite for long-term, flow-mediated structural realignment, the results suggest that the initial response of ECs to an acute change in fluid shear stress is to extend their periphery via actin bursts in the non-upstream directions (25-27). The polymerization of actin to produce these dynamic peripheral edge structures is regulated by the small GTPase Rac (28). Rac pull-down assays revealed that shear stress forces cause a transient upregulation of Rac activity within minutes in subconfluent cells (27). The timing of flow-mediated peripheral remodeling observed here matches with this Rac activity. In addition, shear stress-induced Rac activity regulation required new integrin-ECM ligand binding in the downstream direction, which conferred directional polarity to cells (29). Thus, the spatial dynamics in ECs after onset of shear stress is likely regulated by the polarization of Rac and integrin binding to extracellular matrix ligands.

In contrast to ECs in subconfluent layers, cells in confluent monolayers did not display prominent edge protrusions and lamella-like extensions after the onset of flow. Shear-dependent upregulation of Rac activity is also transient in confluent cell layers (29), and it is also required for the formation and strengthening of cadherin-dependent intercellular adhesion (30-33). Thus, when confluent monolayers were exposed to shear stress, the resultant upregulation in Rac activity may have served a dual role: (1) to prevent indirectly dramatic peripheral movements by strengthening cell-cell adhesions and (2) to induce actin bursts in the edge regions where cell-cell adhesion is not tightly maintained. The latter case is supported by our observation of subtle actin fluctuations at the cell periphery, which indicate that not all the borders between confluent cells are tightly sealed. The nature of these rapid, flow-induced actin bursts suggest the hypothesis that prominent periphery extension is a key part of an endothelial cell's "early-phase flow sensing mechanism" that determines whether to migrate (e.g. subconfluent cells, cells near a wound) or to undergo remodeling/realignment (confluent monolayers). The ability of individual endothelial cells to generate actin bursts in response to flow may act as a signal for them to become directionally polarized and to migrate in the direction of flow. In contrast, the prevention of similar flow-induced actin dynamics in confluent monolayers may cause those cells to go into a period of long-term adaptation that includes morphological realignment and adaptation of gene expression profiles.

Activation of GFP-actin edge activity requires shear stress, since relative cell area remained constant under no-flow conditions. In all cases tested, the slope of the relative cell area with respect

to time was not significantly different from zero. Small trends indicated systematic measurement errors that were most likely due primarily to the low signal-to-noise ratio necessary for live-cell imaging of GFP-actin at this sampling frequency.

One way to test whether the actin dynamics indeed were mediating flow-induced edge activity was to disrupt polymerization (34, 35). In order to preserve the basic structure of cells during the experiments, we chose a low concentration of 0.05 μM cytochalasin D. When ECs in subconfluent layers were exposed to flow with cytochalasin D, their relative cell area increased transiently on a similar time scale to that without cytochalasin D, indicating that part of the spreading response to flow onset is not affected by filament capping. The directional polarization of actin bursts appeared more pronounced with cytochalasin D, as indicated by increased GFP-actin area in the upstream region. Although disruption of dendritic nucleation near ruffling edges would be expected in the presence of cytochalasin D, it is not clear how such directionality would be established in the presence of unidirectional shear stress. Cytochalasin D has been suggested to diminish viscoelastic moduli and structural resistance against applied flow and to disrupt cell-substrate adhesions by preventing actin polymerization (36, 37). Such disruption of the actin-integrin-extracellular matrix association and suppression of flow-mediated Rac upregulation may be expected to lead to the reduced actin response observed here (38). Furthermore, this loss of structural resistance may have caused upstream regions of the cell to be displaced passively in the direction of flow or retracted by elastic prestress forces as the connection between actin and substrate anchors weakened. In subconfluent layers, another possibility is that transient upregulation of Rho-mediated contractility occurred after onset of shear stress that promoted active contractility (27). However, it seems likely that cytochalasin D would prevent Rho-mediated contractility in the presence of cytochalasin D, and the decreased relative cell area after flow onset is more likely to be due to a passive structural collapse in the presence of increased extracellular force.

When confluent monolayers of ECs were subjected to shear stress in the presence of cytochalasin D, cells exhibited a synchronized activity which caused a small but non-significant increase in relative cell area followed by a plateau interval. Several reports have demonstrated that cytochalasin D destabilizes the anchorage between vascular endothelial cadherin and the actin cytoskeleton and disrupts cell-cell adhesions (39-41). Thus, we speculate that cytochalasin D weakened the mechanical stability of adherens junctions and promoted flow-induced displacement of edge-associated actin. Once the cell boundaries became loose, GFP-actin bursts did not likely extend into adjacent cells but rather produced actin "edge explorations" above or below adjacent cells, since the relatively compact monolayer configuration was still present. Two possibilities may explain the rapid flattening of the relative cell area curve: (1) the maximum level of actin polymerization was low, either due to suppression of Rac upregulation or due to filament capping by cytochalasin D, or (2) the degree of cell-cell separation limited further area expansion. If the second hypothesis were true, increased cell edge spreading might be expected in the presence of cytochalasin D because of reduced mechanical modulus. Since this did not occur and the time scale of these measurements was likely too slow to isolate passive deformation from active cellular processes, we suggest that the modification in actin dynamics near the cell edge involved re-balancing of Rac-mediated polymerization dynamics and Rho-mediated contractility. This hypothesis remains to be investigated.

If flow-induced cell edge activity is indeed the result of passive deformation only, then the degree of edge spreading would be expected to depend on the magnitude of shear stress. However, the relative cell area in response to 1 dyn/cm^2 was not significantly different than that in response to 15 dyn/cm^2. Furthermore, increasing the shear stress from 1 dyn/cm^2 to 15 dyn/cm^2 at the time of maximum spreading did not cause an additional increase in relative cell area, suggesting that an active signaling mechanism was saturated or desensitized to additional increases in force magnitude.

In addition, the temporal profile of relative cell area is shear stress magnitude independent. Cells responded to both 1 dyn/cm^2 and 15 dyn/cm^2 by increasing their area for about 12 min and then gradually recovering.

Taken together, the measurements presented here implicate a balance of Rac- and Rho-dependent pathways in rapidly guiding actin remodeling in response to fluid shear stress. Mechanical cues associated with onset of shear stress induce differential actin-mediated morphological changes that are dependent on the monolayer organization, and these rapid phenomena suggest that the actin cytoskeleton serves as a primary integrator in flow sensing mechanisms of cellular mechanotransduction.

Acknowledgement: The authors thank Peter Davies (Univ. of Pennsylvania) for a kind gift of EGFP-actin plasmid. This work was supported by NSF MRSEC for Nanoscopic Materials Design (DMR-0080016), by Whitaker Foundation grant RG-02-0545, and by NIH grant HL-071958.

References

1. Davies PF (1995) *Physiol. Rev.* **75,** 519-560.
2. Dewey CF, Jr., Bussolari SR, Gimbrone MA, Jr., & Davies PF (1981) *J. Biomech. Eng.* **103,** 177-188.
3. Langille BL & O'Donnell F (1986) *Science* **231,** 405-407.
4. Ross R (1999) *New Engl. J. Med.* **340,** 115-126.
5. Caro CG, Fitz-Gerald JM, & Schroter RC (1969) *Nature* **223,** 1159-1161.
6. Zarins CK, Giddens DP, Bharadvaj BK, Sottiurai VS, Mabon RF, & Glagov S (1983) *Circ. Res.* **53,** 502-514.
7. Chien S, Li S, & Shyy YJ (1998) *Hypertension* **31,** 162-169.
8. Galbraith CG, Skalak R, & Chien S (1998) *Cell Motil. Cytoskel.* **40,** 317-330.
9. Ishida T, Takahashi M, Corson MA, & Berk BC (1997) *Ann. NY Acad. Sci.* **811,** 12-23.
10. Nerem RM, Levesque MJ, & Cornhill JF (1981) *J. Biomech. Eng.* **103,** 172-177.
11. Resnick N & Gimbrone MA, Jr. (1995) *FASEB Journal* **9,** 874-882.
12. Davies PF, Barbee KA, Volin MV, Robotewskyj A, Chen J, Joseph L, Griem ML, Wernick MN, Jacobs E, Polacek DC*, et al.* (1997) *Annu. Rev. Physiol.* **59,** 527-549.
13. Franke RP, Grafe M, Schnittler H, Seiffge D, Mittermayer C, & Drenckhahn D (1984) *Nature* **307,** 648-649.
14. Levesque MJ & Nerem RM (1985) *J. Biomech. Eng.* **107,** 341-347.
15. Noria S, Xu F, McCue S, Jones M, Gotlieb AI, & Langille BL (2004) *Am. J. Pathol.* **164,** 1211-1223.
16. Schnittler H-J, Schneider S, Raifer H, Luo F, Dieterich P, Just I, & Aktories K (2001) *Pflügers Archiv European Journal of Physiology* **442,** 675-687.
17. Wechezak AR, Viggers RF, & Sauvage LR (1985) *Lab. Invest.* **53,** 639-647.
18. Burridge K, Fath K, Kelly T, Nuckolls G, & Turner C (1988) *Annual Review of Cell Biology* **4,** 487-525.
19. Maniotis AJ, Chen CS, & Ingber DE (1997) *Proc. Natl Acad. Sci. USA* **94,** 849-854.
20. Helmke BP, Goldman RD, & Davies PF (2000) *Circ. Res.* **86,** 745-752.
21. Helmke BP, Thakker DB, Goldman RD, & Davies PF (2001) *Biophys. J.* **80,** 184-194.
22. Kam Z, Jones MO, Chen H, Agard DA, & Sedat JW (1993) *Bioimaging* **1,** 71-81.
23. Abramoff MD, Magelhaes PJ, & Ram SJ (2004) *Biophotonics Intl* **11,** 36-42.
24. Helmke BP, Rosen AB, & Davies PF (2003) *Biophys. J.* **84,** 2691-2699.

25. Li S, Butler PJ, Wang Y, Hu Y, Han DC, Usami S, Guan J-L, & Chien S (2002) *Proc. Natl Acad. Sci. USA* **99,** 3546-3551.

26. Masuda M & Fujiwara K (1993) *Biol. Cell* **77,** 237-245.

27. Wojciak-Stothard B & Ridley AJ (2003) *J. Cell Biol.* **161,** 429-439.

28. Ridley AJ, Paterson HF, Johnston CL, Diekmann D, & Hall A (1992) *Cell* **70,** 401-410.

29. Tzima E, del Pozo MA, Kiosses WB, Mohamed SA, Li S, Chien S, & Schwartz MA (2002) *EMBO J.* **21,** 6791-6800.

30. Braga VMM, Machesky LM, Hall A, & Hotchin NA (1997) *J. Cell Biol.* **137,** 1421-1431.

31. Breviario F, Caveda L, Corada M, Martin-Padura I, Navarro P, Golay J, Introna M, Gulino D, Lampugnani MG, & Dejana E (1995) *Arterioscler. Thromb. Vasc. Biol.* **15,** 1229-1239.

32. Navarro P, Ruco L, & Dejana E (1998) *J. Cell Biol.* **140,** 1475-1484.

33. Takaishi K, Sasaki T, Kotani H, Nishioka H, & Takai Y (1997) *J. Cell Biol.* **139,** 1047-1059.

34. Cooper JA (1987) *J. Cell Biol.* **105,** 1473-1478.

35. Goddette DW & Frieden C (1986) *J. Biol. Chem.* **261,** 15974-15980.

36. Malek AM & Izumo S (1996) *J. Cell Sci.* **109,** 713-726.

37. Wechezak AR, Wight TN, Viggers RF, & Sauvage LR (1989) *J. Cell. Physiol.* **139,** 136-146.

38. Schwartz MA & Shattil SJ (2000) *Trends in Biochemical Sciences* **25,** 388-391.

39. Baumgartner W, Schutz GJ, Wiegand J, Golenhofen N, & Drenckhahn D (2003) *J. Cell Sci.* **116,** 1001-1011.

40. Castilla MA, Arroyo MVA, Aceituno E, Aragoncillo P, Gonzalez-Pacheco FR, Texeiro E, Bragado R, & Caramelo C (1999) *Circ. Res.* **85,** 1132-1138.

41. Waschke J, Baumgartner W, Adamson RH, Zeng M, Aktories K, Barth H, Wilde C, Curry FE, & Drenckhahn D (2004) *Am. J. Physiol.* **286,** H394-H401.